Geophysical Research Letters

RESEARCH LETTER
10.1029/2018GL079708

Key Points:
- First evidence of rain signature in GNSS Reflectometry observations enabling the technique to detect rain over oceans induced by weak winds
- A novel physical explanation of L-band forward scattering by small-scale ocean surface waves generated by raindrop splashes
- Reduction in the value of GNSS-R Bistatic radar cross section during rain events

Correspondence to:
M. Asgarimehr,
milad.asgarimehr@gfz-potsdam.de

Citation:
Asgarimehr, M., Zavorotny, V., Wickert, J., & Reich, S. (2018). Can GNSS Reflectometry detect precipitation over oceans? *Geophysical Research Letters*, *45*, 12,585–12,592. https://doi.org/10.1029/2018GL079708

Received 20 JUL 2018
Accepted 1 NOV 2018
Accepted article online 6 NOV 2018
Published online 20 NOV 2018

Can GNSS Reflectometry Detect Precipitation Over Oceans?

Milad Asgarimehr[1,2], Valery Zavorotny[3,4], Jens Wickert[1,2], and Sebastian Reich[5]

[1]Institute of Geodesy and Geoinformation Science, Faculty VI, Technische Universität Berlin, Berlin, Germany, [2]German Research Centre for Geosciences GFZ, Potsdam, Germany, [3]Cooperative Institute for Research in Environmental Sciences, University of Colorado Boulder, Boulder, CO, USA, [4]Earth System Research Laboratory, NOAA, Boulder, CO, USA, [5]Department of Mathematics, University of Potsdam, Potsdam, Germany

Abstract For the first time, a rain signature in Global Navigation Satellite System Reflectometry (GNSS-R) observations is demonstrated. Based on the argument that the forward quasi-specular scattering relies upon surface gravity waves with lengths larger than several wavelengths of the reflected signal, a commonly made conclusion is that the scatterometric GNSS-R measurements are not sensitive to the surface small-scale roughness generated by raindrops impinging on the ocean surface. On the contrary, this study presents an evidence that the bistatic radar cross section σ^0 derived from TechDemoSat-1 data is reduced due to rain at weak winds, lower than $\approx$ 6 m/s. The decrease is as large as $\approx$ 0.7 dB at the wind speed of 3 m/s due to a precipitation of 0–2 mm/hr. The simulations based on the recently published scattering theory provide a plausible explanation for this phenomenon which potentially enables the GNSS-R technique to detect precipitation over oceans at low winds.

Plain Language Summary Using Global Navigation Satellite System (GNSS) signals, reflected off the Earth's surface (GNSS Reflectometry), is an innovative remote sensing technique with a broad spectrum of geophysical applications. Currently, recent satellite missions, such as the U.K. TechDemoSat-1 and U.S. Cyclone Global Navigation Satellite System (CYGNSS), pioneer GNSS Reflectometry as a new space observation technology on a global scale. Despite a wide variety of monitored geophysical parameters, the reflected signals have never been used to obtain rain information. For the first time, this study demonstrates a signature in the received signals, due to the modified ocean surface waves by rain splashes, enabling the technique to detect precipitation over oceans induced by weak winds. A plausible physical explanation for this phenomenon is provided based on the recent scattering theory. This study can serve as a starting point for developing a new GNSS Reflectometry application, rain detection over oceans, which might be also implemented for future low-cost GNSS remote sensing missions. The presented findings also provide a better physical understanding of L band forward scattering mechanism which is directly relevant to the main objective of the currently operational GNSS Reflectometry satellite missions.

1. Introduction

Over the last two decades, there has been a rapidly growing interest in the use of Global Navigation Satellite System (GNSS) signals reflection from the Earth's surface to monitor a variety of geophysical parameters (see, e.g., Jin et al., 2014; Zavorotny et al., 2014). Despite a wide variety of GNSS Reflectometry (GNSS-R) applications for Earth's systems monitoring, the reflected signals have been hardly considered as a potential rain indicator due to lack of both experimental evidence and theoretical substantiation of such a phenomenon. Indeed, it is commonly assumed that GNSS is an all-weather system due to the fact that frequencies for the GNSS signals are chosen in the L band, so they would not suffer noticeable attenuation by clouds or typical precipitation, and as a result, they are not sensitive to rain. However, the sensitivity to rain might not be limited only to rain attenuation caused by signal absorption in drops and accompanying scattering. Other signal propagation effects may be involved. For example, Cardellach et al. (2015) recently proposed to use a depolarization effect induced by the flattening of the heavy precipitation drops to detect heavy rains.

The surface effects of precipitation on microwave wind scatterometry have been known already for several decades, and they are well documented (Braun et al., 2002; Cavaleri et al., 2015; Contreras & Plant, 2006; Contreras et al., 2003; Craeye et al., 1997; 1999; Hansen, 1986; Hwang, 2012; Melsheimer et al., 1998; 2001; Milliff et al., 2004; Moore et al., 1979; Nie & Long, 2007; Portabella et al., 2012; Sobieski et al., 1999; Weissman

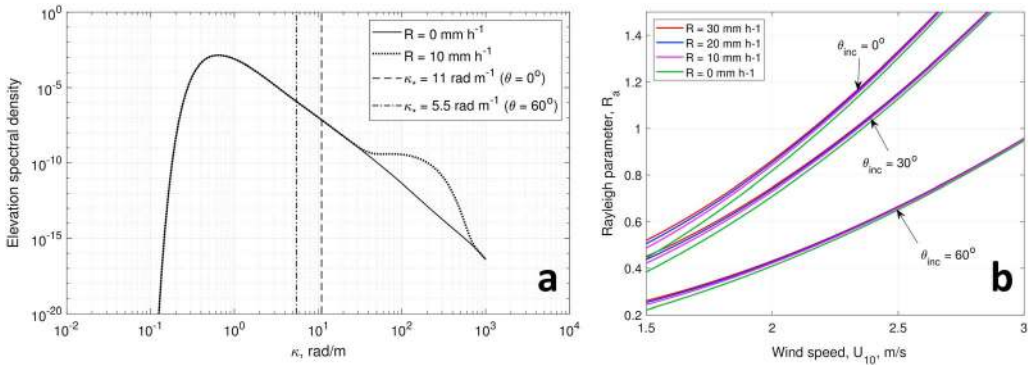

Figure 1. Wave elevation spectrum (a) at wind speed 3 m/s without rain and modified by rain (rain rate R = 10 mm/hr) along with the k_* for incidence angles of 0° and 60° shown with vertical dashed and dash-dotted lines and surface roughness Rayleigh parameter R_a (b) versus wind speed for a range of rain rates and for three incidence angles θ_{inc}.

et al., 2002, 2012). These effects can be explained by the following impact model. Drops strike the water surface producing splashes which, in its turn, generate gravity-capillary ring waves from which the microwave signal scatters. The additional ocean surface roughening can be described in terms of the modified wave elevation spectrum. Naturally, such a roughening effect can be mostly noticed at low wind speeds when heights of wind-generated waves are relatively low.

With the emergence of the GNSS bistatic radar ocean forward scatterometry a question has been posed: Can rain surface effects have a similar impact on the GNSS reflected signals? It is clear that this case requires a special consideration because the mechanism of L band forward scattering significantly differs from microwave backscattering implemented in traditional wind scatterometry. Ghavidel and Camps (2016) investigated a GNSS-R electromagnetic bias due to the rain and also by swell and sea currents performing numerical simulations; however, the rain sensitivity of GNSS wind scatterometry was not addressed in that publication. Soisuvarn et al. (2016) analyzed a limited GNSS-R data set under rain conditions obtained during the UK TechDemoSat-1 (TDS-1) mission. Although some spread for the signal-to-noise-ratio (SNR) at different rain rates is shown in this study, the authors draw no conclusion whether or not there is any effect of rain on GNSS-R measurements and defer it until a substantially larger data set for statistical analysis is available. Currently, TDS-1 has provided a significantly larger data set being operational for a longer time. Consequently, a noticeably larger number of observations, especially at higher rain rates, are investigated in this study.

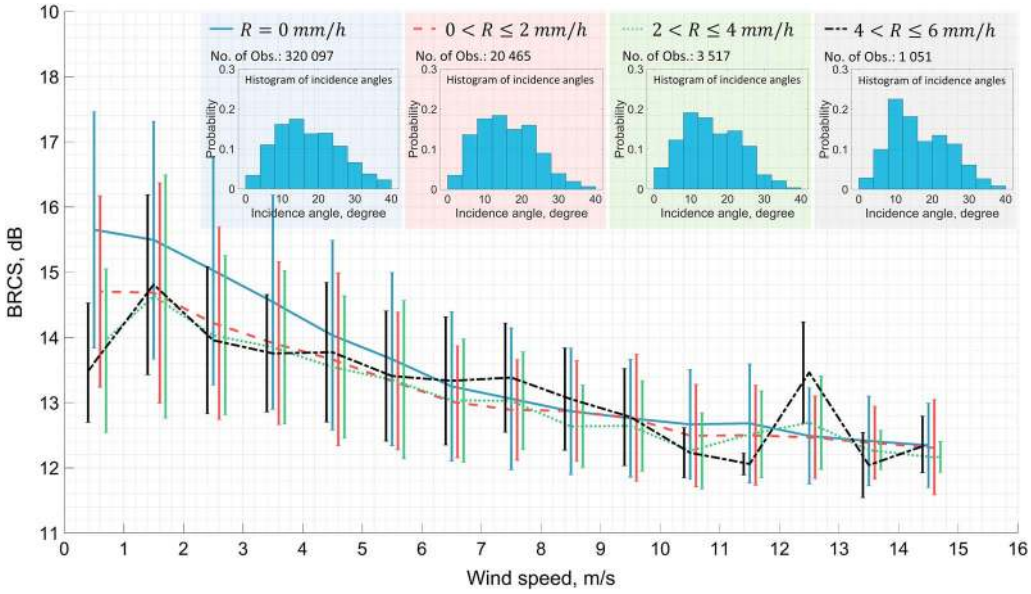

Figure 2. BRCS σ^0 versus wind speed at different rain rates R (mm/hr) along with the number of observations and the histogram of incidence angles for the measurements in each rain rate bin. BRCS = bistatic radar cross section.

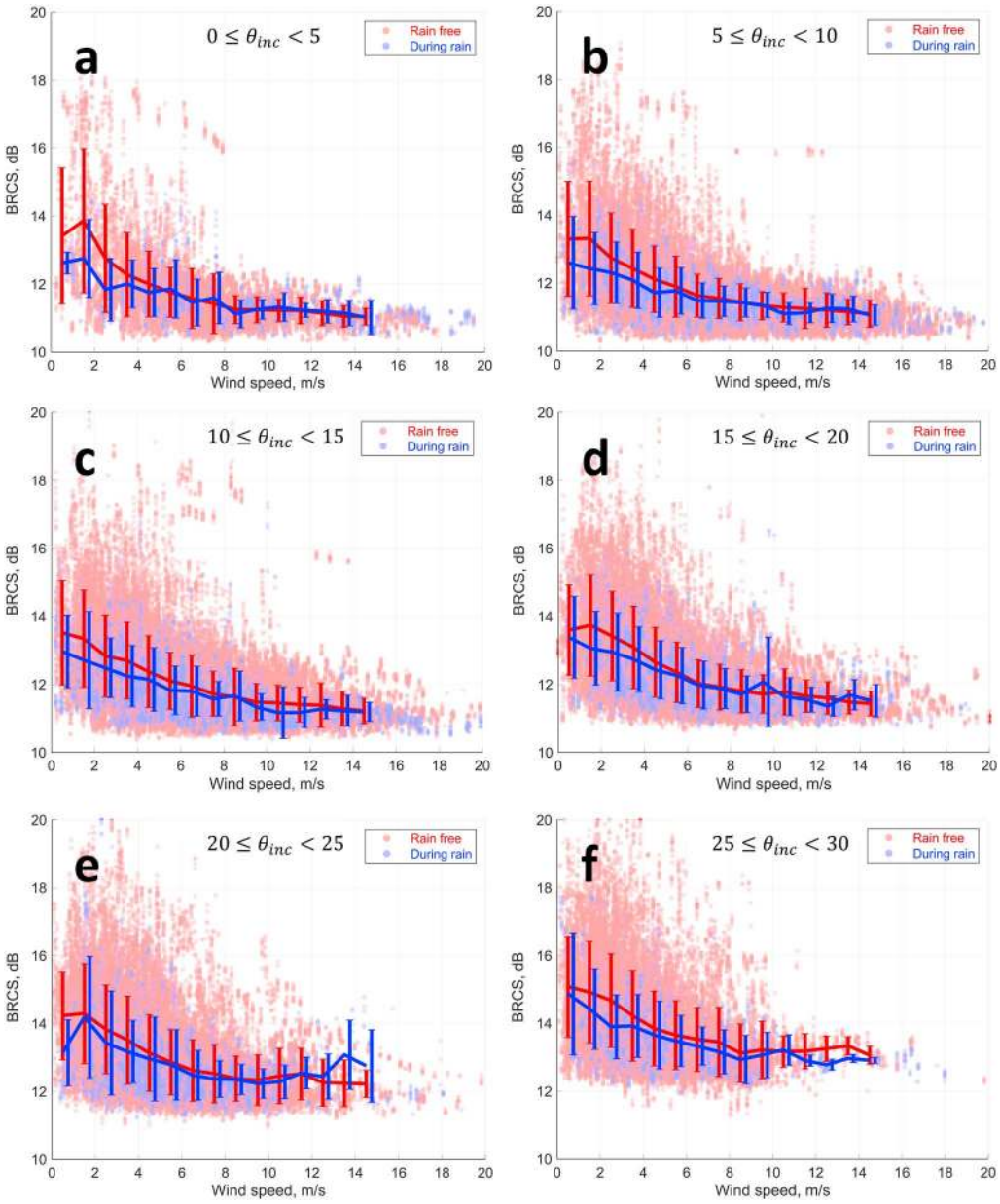

Figure 3. BRCS versus wind speed at different incidence angles: $0° \le \theta_{inc} < 5°$ (a), $5° \le \theta_{inc} < 10°$ (b), $10° \le \theta_{inc} < 15°$ (c), $15° \le \theta_{inc} < 20°$ (d), $20° \le \theta_{inc} < 25°$ (e), and $25° \le \theta_{inc} < 30°$ (f). BRCS = bistatic radar cross section.

At first glance, the GNSS reflected signal should not be sensitive to gravity-capillary waves generated by drop splashes because of the nature of the forward quasi-specular scattering. Indeed, according to the model presented by Zavorotny and Voronovich (2000), the surface parameter that controls the intensity of forward quasi-specular scattering is the low-pass mean square slope, MSS_{LP}, of the ocean surface. It is determined by the part of the wave slope spectrum that resides at wave numbers smaller than $k_* = k \cos\theta_{inc}/3$, where θ_{inc} is an incidence angle and k is the wave number $(2\pi/\lambda)$ of the L band GNSS signal.

Figure 1a demonstrates a wave elevation spectrum (Elfouhaily et al., 1997) induced by a wind speed of 3 m/s, together with the log Gaussian spectrum (Craeye et al., 1997) used to describe the rain-induced ring waves at rain rates of 10 mm/hr. As seen from this plot, the part of the spectrum affected by rain splashes resides at wave numbers much higher than cutoff number k_*, which is $\approx$ 11 rad/m for $\theta_{inc} = 0°$ and $\approx$ 5.5 rad/m for $\theta_{inc} = 60°$. However, the type of scattering described by Zavorotny and Voronovich (2000; also known as a strong diffuse scattering) takes place for rough surfaces with a high enough ($\gg$ 1) Rayleigh parameter,

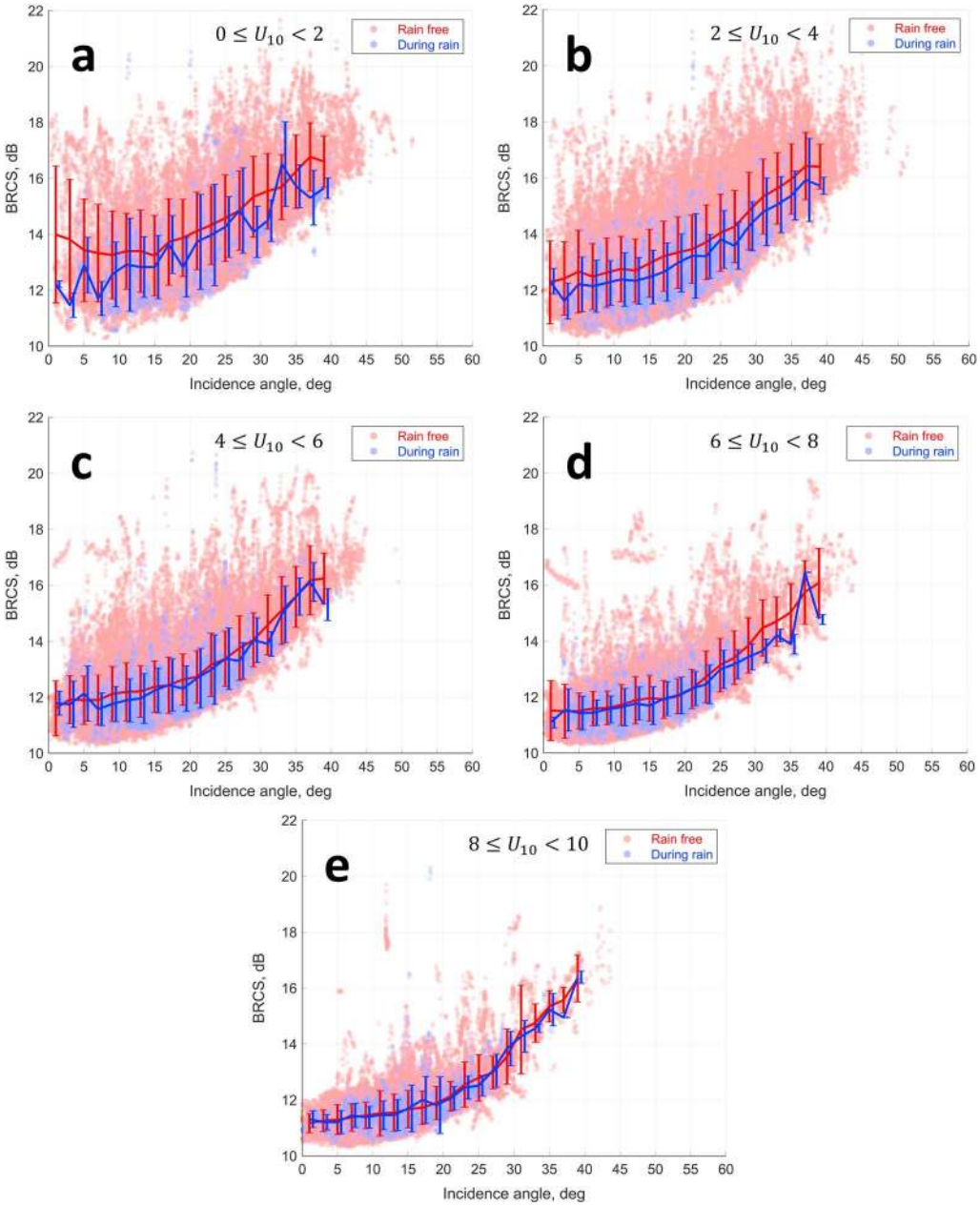

Figure 4. BRCS versus the incidence angle at different wind speeds: $0 \le U_{10} < 2$ m/s (a), $2 \le U_{10} < 4$ m/s (b), $4 \le U_{10} < 6$ m/s (c), $6 \le U_{10} < 8$ m/s (d), and $8 \le U_{10} < 10$ m/s (e). BRCS = bistatic radar cross section.

$R_a = kh\cos\theta_{\mathrm{inc}}$, where h is the root-mean-square of surface heights. At such conditions, the forward bistatic scattering can be described by the geometric optics approximation which involves surface slopes of waves with wave numbers smaller than k_* as described above. For typical ocean conditions, this happens for winds with speed $U_{10} > 4-5$ m/s. For weaker winds (and, respectively, $R_a \le 1$) the scattering mechanism changes. Instead of quasi-specular scattering, driven by surface slopes, it becomes more like a higher-order Bragg scattering, driven by parameter R_a. Since R_a is proportional to h, which in its turn results from integrating the entire surface elevation spectrum, it also includes the spectral interval affected by rain splashes. Voronovich and Zavorotny (2017) proposed a bistatic scattering model that describes such a weak diffuse scattering providing a smooth transition to the regime of strong diffuse scattering. For weak enough winds, the magnitude of the spectral peak due to wind-generated waves becomes comparable to the one of the secondary peak due to the rain-generated ring waves. As a result, the root-mean-square of surface heights (and, therefore,

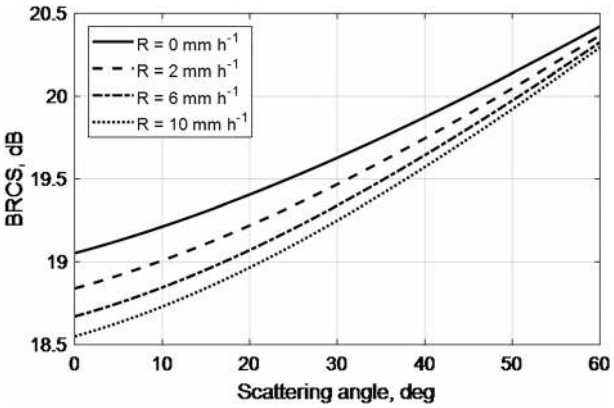

Figure 5. BRCS σ^0 versus the scattering angle for U_{10} = 3 m/s at different rain rates R. BRCS = bistatic radar cross section.

the Rayleigh parameter) becomes sensitive to the rain-generated ring waves. Figure 1b shows R_a versus the wind speeds between 1.5 and 3 m/s and how it responds to a range of rain rates at incidence angles of 0°, 30°, and 60°.

In this study, for the first time, the sensitivity of GNSS-R observations to the rain splash effect, in terms of changes in the bistatic radar cross section (BRCS), is discussed. The investigation is conducted using both the data from TDS-1 and simulations based on the scattering model (Voronovich & Zavorotny, 2017). Section 2 briefly describes the used data, whereas, in section 3, the rain effect on the real observations is demonstrated. Section 4 discusses the model-based simulations. Finally, the concluding remarks are presented.

2. Data Description

GNSS-R measurements of TDS-1 are analyzed in this study. The Level 1b data covering the temporal interval from June 2015 to July 2017 are used. The ice-affected ocean observations whose latitude is above 55° (or below −55°), as well as measurements with a negative SNR (< 0 dB), are omitted from the analyses. The data are available to the users by the Measurement of Earth-Reflected Radio navigation Signals By Satellite. For each observation, BRCS σ^0 is computed using the bistatic radar equation (Zavorotny & Voronovich, 2000) and as described by Foti et al. (2015).

ERA-Interim reanalysis measurements, based on the Integrated Forecast System European Centre for Medium-Range Weather Forecasts (ECMWF) model, are used as the match-up data set in this study. The model winds are analyzed by a four-dimensional variational analysis with a 12-hr analysis window. The reanalysis assimilates data from various sources including satellite and ground-based observations (Dee et al., 2011). Six-hourly data with a spatial resolution of 0.75° are used. For TDS-1, σ^0 was computed from the peak zone of the Doppler-delay map (DDM) corresponding to a spatial resolution between 22 and 30 km (median value 25 km) depending on the incidence angle of the specular point (see, e. g., Unwin et al., 2016). The derived TDS-1 BRCSs are collocated both spatially and temporally within 60 km and 30 min, and the resultant measurements are analyzed.

The precipitation value of each TDS-1/ERA-Interim measurement is obtained from 3-hourly combined Level 3 microwave-IR estimates (3B42 Version 7) of The Tropical Rainfall Measuring Mission (TRMM). The TRMM 3B42 product is obtained from TRMM merged with other satellite measurements. This data set has a 3-hr temporal and 0.25° spatial resolution and covers from 60°S to 60°N (Huffman & Bolvin, 2015), which consequently meets the requirements for the analyses in this study. However, global precipitation measurement alternatively provides half-hourly Level 3 R estimates with a higher spatial resolution of 0.1°, which can be also used for future studies (Huffman et al., 2015). Finally, the data collocation results in 346,091 measurements from which 25,994 observations are collected during precipitation. To be more specific, 20,465, 3,517, and 1,051 measurements are at rain rates 0–2, 2–4, and 4–6 mm/hr, respectively, and the rest are at higher rates.

Considering the current level of retrieval uncertainty and the spatiotemporal resolution of spaceborne GNSS-R, and the fact that this study is the first and preliminary demonstration of rain detection feasibility using this technique, one can be satisfied with the above data sets for rain signature analyses. However, future studies might consider other phenomena affecting the GNSS-R measurements such as swell and wave age by incorporating the wave information from wave observations or models such as the National Oceanic and Atmospheric Administration Wavewatch III® (Tolman, 2009). We cannot exclude a possibility that some other processes are involved such as ocean surface roughening by air downdrafts (Weissman et al., 2012). At the same time, spatial inhomogeneity of rain and wind speed in the low wind speed regime, so-called light and variable winds, can be potentially studied, but the current spatial resolution of the GNSS-R technique is too coarse to resolve a spatial structure of wind and precipitation. Accordingly, this study stays satisfied with the preliminary objective of showing the existence of rain signature, while future investigations may include the quantitative analyses of potential phenomena using CYGNSS measurements.

3. Rain Signatures in TDS-1 Measurements

Figure 2, demonstrates the average derived BRCS versus wind speed U_{10}. The figure shows a systematic decrease in BRCS due to rain at winds weaker than ≈ 6 m/s. At wind speeds lower than 2 m/s, the difference

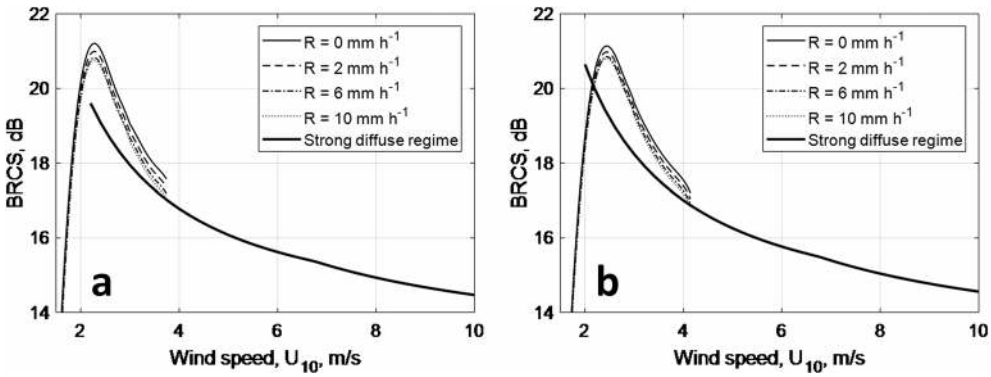

Figure 6. BRCS σ^0 versus wind speed for scattering angles of 0° (a) and 30° (b) at different rain rates R. BRCS = bistatic radar cross section.

between obtained σ^0 during rain and the one derived in a rain-free environment becomes greater in size as the rain rate increases. The curves corresponding to different rain rates converge each other at the wind speed of almost 6 m/s, showing no significant difference.

In Figure 3, the data are divided into six groups of different incidence angles. The BRCS in the rain-free area (red) and during rain events (blue) are shown versus the wind speed. Accordingly, the decrease in BRCS persists at any range of incidence angles. In addition, BRCS versus the incidence angle is shown by Figure 4 splitting the data into five groups of wind speed severity. The decrease in BRCS is evident for first two groups, $U_{10} < 2$ m/s and $2 \leq U_{10} < 4$. An artificial upward trend is also observed which is due to the omission of the data with insufficient quality, which means observations with negative SNRs here.

According to the discussed results in this section, the change in BRCS due to rain is significantly evident. This change is such that, as shown in Figure 2, at a wind speed of less than 2 m/s, BRCS is dropped as large as almost 1 dB due to a precipitation of 0–2 mm/hr. The results demonstrate that BRCS is independent of rain at winds higher than almost 6 m/s which is shown in Figures 2 and 3 as well as 4c–4e. The analysis is not able to reveal how the rain effect changes in size at different incidence angles due to the existing inaccuracies.

4. Model-Based Simulations

Based on the scattering model from Voronovich and Zavorotny (2017), which used the small slope approximation of the first order, the surface effect of rain on L band BRCS can be expected only at weak diffuse scattering. Indeed, numerical simulations using this scattering model demonstrate that there is a sensitivity of the BRCS, σ^0, to various rainfall rates for a range of low wind speeds. In these simulations, the wave spectrum from Elfouhaily et al. (1997) was used for the case of fully developed seas. Results of simulations are presented in Figures 5 and 6.

The dependence of modeled BRCS in a nominal specular direction for various rainfall rates R as a function of the incidence/scattering angle at $U_{10} = 3$ m/s is shown in Figure 5. It is seen that sensitivity of the BRCS to the surface rain effect reduces with the scattering angle. The dependence of modeled BRCS in a nominal specular direction for various rainfall rates R as a function of wind speed for the incidence/scattering angles of 0° and 30° is shown in Figure 6. The thin lines at winds below 4 m/s are obtained using the scattering model from Voronovich and Zavorotny (2017), whereas the thick solid lines represent the result valid for the regime of strong diffuse scattering, such as in Zavorotny and Voronovich (2000). It is seen that being accurate for high winds, these curves at winds below 4 m/s underestimate the true σ^0 dependence on wind speed. They do not show any sensitivity to the rain rate for the entire range of winds as well.

It should be noted that, for the case of $R_a \leq 1$, together with a diffuse incoherent component, a coherent component emerges. However, because of a strong effect of the decorrelation factor $\exp(-4R_a^2)$, the coherent component can be neglected for winds $U_{10} > 2$ m/s according to the modeling results presented by Zavorotny and Voronovich (2018). They show that the coherent component is, to some extent, sensitive to rain, but it decays very fast as the Rayleigh parameter grows above 1, yielding to the incoherent component.

5. Discussion and Conclusions

A possible rain effect on TDS-1 GNSS-R data was studied. The analysis of the data demonstrated a significant decrease in the BRCS during rain events at winds weaker than ≈ 6 m/s. At a wind speed of 3 m/s, the average decrease in the BRCS is about 0.7 dB due to precipitations of 0–2 mm/hr. The reduction is almost 1 dB for winds weaker than 2 m/s at the same rain rates. The decrease in the BRCS persists at any range of incidence angles; however, the rain effect might vary in size at different incidence angles which cannot be well seen due to existing noise and various uncertainties in the observations.

The simulations qualitatively predict similar trends in the BRCS dependencies on wind speed and the incidence angle for various rain rates in the range of low wind speeds. The sensitivity of the modeled BRCS curves to changes in rain rate for the interval of weak winds is due the fact that the BRCS for such wind conditions is controlled by the surface Rayleigh parameter rather than by the L band low-pass mean square slope. Our modeling study predicts this phenomenon only for the low wind speeds, below 4–5 m/s, which are not that rare on the global scale since the median global wind speed is around 6 m/s. A presence of swell probably can diminish the rain effect on the BRCS, but the limitations of the numerical scheme used here did not allow us to model the influence of swell. For wind speeds higher than 4–5 m/s the previous strongly diffuse (quasi-specular) scattering model is still valid. As expected, it does not demonstrate any sensitivity to the precipitation.

From the comparison between the measured and modeled BRCS it is seen that there is no exact quantitative match between them. This is mainly due to the limitations imposed by the data uncertainties and current spatiotemporal resolution of the measurements, as well as due to existence of other oceanic phenomena affecting the retrieved BRCS discussed in section 2. On the other hand, the model for the rain-modified spectrum is rather simplistic and is not fully validated for field conditions, so it might be subject to some refinements. Overall, the modeling results demonstrate that the observed BRCS sensitivity to precipitation does not contradict the physics of bistatic forward scattering of the GNSS signals at weak winds and, moreover, can be qualitatively explained by the ocean surface roughening due to raindrop splashes. As a result, one can conclude from this study that rain can be detected by GNSS-R observations at weak winds.

Acknowledgments
This publication was financially supported by Geo.X, the Research Network for Geosciences in Berlin and Potsdam. We thank the TDS-1 team at Surrey Satellite Technology Ltd for providing TDS-1 data as well as the teams associated with ECMWF and TRMM. All the data used in this study are publicly available and free of charge.

References

Braun, N., Gade, M., & Lange, P. (2002). The effect of artificial rain on wave spectra and multi-polarisation X band radar backscatter. *International Journal of Remote Sensing*, *23*(20), 4305–4323.

Cardellach, E., Tomás, S., Oliveras, S., Padullés, R., Rius, A., de la Torre-Juárez, M., et al. (2015). Sensitivity of PAZ LEO polarimetric GNSS radio-occultation experiment to precipitation events. *IEEE Transactions on Geoscience and Remote Sensing*, *53*(1), 190–206.

Cavaleri, L., Bertotti, L., & Bidlot, J.-R. (2015). Waving in the rain. *Journal of Geophysical Research: Oceans*, *120*, 3248–3260. https://doi.org/10.1002/2014JC010348

Contreras, R. F., & Plant, W. J. (2006). Surface effect of rain on microwave backscatter from the ocean: Measurements and modeling. *Journal of Geophysical Research*, *111*, C08019. https://doi.org/10.1029/2005JC003356

Contreras, R. F., Plant, W. J., Keller, W. C., Hayes, K., & Nystuen, J. (2003). Effects of rain on ku-band backscatter from the ocean. *Journal of Geophysical Research*, *108*(C5), 3165. https://doi.org/10.1029/2001JC001255

Craeye, C., Sobieski, P., & Bliven, L. (1997). Scattering by artificial wind and rain roughened water surfaces at oblique incidences. *International Journal of Remote Sensing*, *18*(10), 2241–2246.

Craeye, C., Sobieski, P. W., Bliven, L. F., & Guissard, A. (1999). Ring-waves generated by water drops impacting on water surfaces at rest. *IEEE Journal of Oceanic Engineering*, *24*(3), 323–332.

Dee, D. P., Uppala, S. M., Simmons, A., Berrisford, P., Poli, P., Kobayashi, S., et al. (2011). The ERA-interim reanalysis: Configuration and performance of the data assimilation system. *Quarterly Journal of the royal meteorological society*, *137*(656), 553–597.

Elfouhaily, T., Chapron, B., Katsaros, K., & Vandemark, D. (1997). A unified directional spectrum for long and short wind-driven waves. *Journal of Geophysical Research*, *102*(C7), 15,781–15,796.

Foti, G., Gommenginger, C., Jales, P., Unwin, M., Shaw, A., Robertson, C., & Rosello, J. (2015). Spaceborne GNSS reflectometry for ocean winds: First results from the UK TechDemoSat-1 mission. *Geophysical Research Letters*, *42*, 5435–5441. https://doi.org/10.1002/2015GL064204

Ghavidel, A., & Camps, A. (2016). Impact of rain, swell, and surface currents on the electromagnetic bias in GNSS-reflectometry. *IEEE Journal of Selected Topics in Applied Earth Observations and Remote Sensing*, *9*(10), 4643–4649.

Hansen, J. (1986). Rain backscatter tests dispel old theories. *Microwaves*, *25*, 97.

Huffman, G. J., & Bolvin, D. T. (2015). Real-time TRMM multi-satellite precipitation analysis data set documentation. NASA Tech. Doc.

Huffman, G. J., Bolvin, D. T., Braithwaite, D., Hsu, K., Joyce, R., Xie, P., & Yoo, S.-H. (2015). NASA global precipitation measurement (GPM) integrated multi-satellite retrievals for GPM (IMERG). *Algorithm Theoretical Basis Document, Version*, *4*, 30.

Hwang, P. A. (2012). Foam and roughness effects on passive microwave remote sensing of the ocean. *IEEE Transactions on Geoscience and Remote Sensing*, *50*(8), 2978–2985.

Jin, S., Cardellach, E., & Xie, F. (2014). *GNSS remote sensing: Theory, methods and applications*. Dordrecht: Springer.

Melsheimer, C., Alpers, W., & Gade, M. (1998). Investigation of multifrequency/multipolarization radar signatures of rain cells over the ocean using SIR-C/X-SAR data. *Journal of Geophysical Research*, *103*(C9), 18,867–18,884.

Melsheimer, C., Alpers, W., & Gade, M. (2001). Simultaneous observations of rain cells over the ocean by the synthetic aperture radar aboard the ERS satellites and by surface-based weather radars. *Journal of Geophysical Research*, *106*(C3), 4665–4677.

Milliff, R. F., Morzel, J., Chelton, D. B., & Freilich, M. H. (2004). Wind stress curl and wind stress divergence biases from rain effects on QSCAT surface wind retrievals. *Journal of Atmospheric and Oceanic Technology*, *21*(8), 1216–1231.

Moore, R., Yu, Y., Fung, A., Kaneko, D., Dome, G., & Werp, R. (1979). Preliminary study of rain effects on radar scattering from water surfaces. *IEEE Journal of Oceanic Engineering*, *4*(1), 31–32.

Nie, C., & Long, D. G. (2007). A C-band wind/rain backscatter model. *IEEE Transactions On Geoscience and Remote Sensing*, *45*(3), 621–631.

Portabella, M., Stoffelen, A., Lin, W., Turiel, A., Verhoef, A., Verspeek, J., & Ballabrera-Poy, J. (2012). Rain effects on ASCAT-retrieved winds: Toward an improved quality control. *IEEE Transactions on Geoscience and Remote Sensing*, *50*(7), 2495–2506.

Sobieski, P. W., Craeye, C., & Bliven, L. F. (1999). Scatterometric signatures of multivariate drop impacts on fresh and salt water surfaces. *International Journal of Remote Sensing*, *20*(11), 2149–2166.

Soisuvarn, S., Jelenak, Z., Said, F., Chang, P. S., & Egido, A. (2016). The GNSS reflectometry response to the ocean surface winds and waves. *IEEE Journal of Selected Topics in Applied Earth Observations and Remote Sensing*, *9*(10), 4678–4699.

Tolman, H. L. (2009). User manual and system documentation of wavewatch III TM version 3.14. *Technical note MMAB Contribution*, *276*, 220.

Unwin, M., Jales, P., Tye, J., Gommenginger, C., Foti, G., & Rosello, J. (2016). Spaceborne GNSS-reflectometry on techDemoSat-1: Early mission operations and exploitation. *IEEE Journal of Selected Topics in Applied Earth Observations and Remote Sensing*, *9*(10), 4525–4539.

Voronovich, A. G., & Zavorotny, V. U. (2017). The transition from weak to strong diffuse radar bistatic scattering from rough ocean surface. *IEEE Transactions on Antennas and Propagation*, *65*(11), 6029–6034.

Weissman, D. E., Bourassa, M. A., & Tongue, J. (2002). Effects of rain rate and wind magnitude on seawinds scatterometer wind speed errors. *Journal of Atmospheric and Oceanic Technology*, *19*(5), 738–746.

Weissman, D., Stiles, B., Hristova-Veleva, S., Long, D., Smith, D., Hilburn, K., & Jones, W. (2012). Challenges to satellite sensors of ocean winds: Addressing precipitation effects. *Journal of Atmospheric and Oceanic Technology*, *29*(3), 356–374.

Zavorotny, V. U., Gleason, S., Cardellach, E., & Camps, A. (2014). Tutorial on remote sensing using GNSS bistatic radar of opportunity. *IEEE Geoscience and Remote Sensing Magazine*, *2*(4), 8–45.

Zavorotny, V. U., & Voronovich, A. G. (2000). Scattering of GPS signals from the ocean with wind remote sensing application. *IEEE Transactions on Geoscience and Remote Sensing*, *38*(2), 951–964.

Zavorotny, V. U., & Voronovich, A. G. (2018). GNSS-R modeling results obtained with improved bistatic radar equation. In *Proceedings of the International Conference on Electromagnetics in Advanced Applications (ICEAA '2018)*, Cartagena, Colombia, pp. 10–14.